P. Masarati, G. Quaranta, A. Bernardini, G. Guglieri
Voluntary Pilot Action Through Biodynamics for Helicopter Flight Dynamics Simulation
Journal of Guidance Control and Dynamics, Vol. 38, N. 3, 2015, p. 431-441
doi:10.2514/1.G000837

Voluntary Pilot Action Through Biodynamics for Helicopter Flight Dynamics Simulation

Pierangelo Masarati*, Giuseppe Quaranta†

Dipartimento di Scienze e Tecnologie Aerospaziali, Politecnico di Milano,

via La Masa 34 20156 Milano, Italy

Andrea Bernardini‡, Giorgio Guglieri§

Dipartimento di Ingegneria Meccanica e Aerospaziale, Politecnico di Torino,

corso Duca degli Abruzzi 24, 10129 Torino, Italy

This work presents the integration of detailed models of a pilot controlling a helicopter along the heave axis through the collective control inceptor. The action on the control inceptor is produced through a biomechanical model of the pilot's limbs, by commanding the activation of the related muscle bundles. Such activation, in turn, is determined by defining the muscle elongations required to move the control inceptor in order to obtain the control of the vehicle according to a high-level model of the voluntary action of the pilot acting as a regulator for the vehicle. The biomechanical model of the pilot's limbs and the aeromechanical model of the helicopter are implemented in a general-purpose multibody simulation. The helicopter model, the biomechanical model of the pilot's limbs, the cognitive model of the pilot and their integration are discussed. The integrated model is applied to the simulation of simple, yet representative mission task elements.

Nomenclature

a	non-dimensional muscular activation
a_{ref}	non-dimensional reference muscular activation

*Associate Professor, Dipartimento di Scienze e Tecnologie Aerospaziali; AIAA member; corresponding author

†Assistant Professor, Dipartimento di Scienze e Tecnologie Aerospaziali

‡Graduate Student, Dipartimento di Ingegneria Meccanica e Aerospaziale

§Associate Professor, Dipartimento di Ingegneria Meccanica e Aerospaziale

b_0	static gain of involuntary pilot model (see $H_{\eta\ddot{z}}(s)$), radian/m
e_z	vertical position error ($e_z = z_d - z$), m
f_m	muscle force, N
f_{m_0}	muscle maximum isometric force, N
f_1, f_2, f_3	non-dimensional configuration-dependent contributions to muscle force
g	gravity acceleration, m/s^2
ℓ	muscle length, m
ℓ_0	reference muscle length, mm
ℓ_d	desired muscle length, m
m_e	friction moment applied to the control inceptor, N·m
p	swashplate actuator time constant (first-order approximation), s
s	Laplace operator, 1/s
t	time, s
v	non-dimensional muscle elongation rate
x	non-dimensional muscle length
x_{ref}	reference non-dimensional muscle length
x_1, x_2	x component of muscle insertion point positions, mm
y_1, y_2	y component of muscle insertion point positions, mm
z	vertical position, m
z_1, z_2	z component of muscle insertion point positions, mm
z_d	desired vertical position, m
A	reference amplitude in vertical maneuver, m
C_1	threshold torque of the simplified control inceptor friction model, N·m
C_2	slope of the simplified control inceptor friction model, s/radian
G	gearing ratio non-dimensional scaling parameter (nominal: $G = 1$)
G_c	gearing ratio between control inceptor and blade pitch rotation, radian/radian
$H_{\text{ff}}(s)$	feedforward control transfer function, radian/m
$H_{\text{L}}(s)$	loop transfer function
$H_{\text{NMD}}(s)$	neuro-muscular electromechanical delay transfer function
$H_{z\theta}(s)$	control to motion transfer function (vehicle model), m/radian
$\hat{H}_{z\theta}(s)$	approximated, low-pass filtered vehicle model, m/radian
$H_{\eta\ddot{z}}(s)$	biodynamic feedthrough transfer function, radian·s^2/m
$H_{\theta e_z}(s)$	error to control transfer function (voluntary pilot model), radian/m
J	inertia of control device, kg·m^2
K_A	pilot's gain (Szabolcsi's pilot model), radian/m
K_d	derivative coefficient of reflexive activation quasi-steady approximation, 1/m

K_p	proportional coefficient of reflexive activation quasi-steady approximation, s/m
M	vehicle mass, kg
T	reference time in vertical maneuver, s
T_1, T_2, T_3	time constants (Szabolcsi's pilot model), s
V_0	reference muscle elongation rate, m/s
Z	net vertical force (main rotor thrust minus weight), N
α_1, α_2	low-pass filter coefficients (used with McRuer's crossover pilot model), s, s^2
η	collective control inceptor rotation, radian
θ	blade collective pitch, radian
ξ_a	swashplate actuator damping factor (second-order approximation)
ξ_f	low-pass filter damping factor
ξ_p	damping factor of involuntary pilot model (see $H_{\eta\ddot{z}}(s)$)
τ_e	equivalent time delay (McRuer's crossover pilot model), s
ω_a	swashplate actuator cut frequency (second-order approximation), radian/s
ω_c	crossover frequency (McRuer's crossover pilot model), radian/s
ω_f	low-pass filter cut frequency, radian/s
ω_p	characteristic frequency of involuntary pilot model (see $H_{\eta\ddot{z}}(s)$), radian/s
$\Delta(\cdot)$	finite perturbation operator
$(\spadesuit)_{/(\clubsuit)}$	partial derivative of ($\spadesuit$) with respect to ($\clubsuit$)

I. Introduction

Pilot-vehicle interaction may impact the operation of vehicles as well as health and even safety of the occupants. This work focuses on specific aspects of pilot-helicopter interaction, addressing diverse fields that include vehicle dynamics and aeroelasticity analysis, pilot biomechanics, and pilot behavioral models. The problem is formalized and analyzed using general-purpose multibody dynamics, which provides the capability to deal with its most important aspects in a monolithic formulation and implementation, with comparable detail levels.

The problem of adverse Aircraft-Pilot Couplings (APCs) surfaced from the very beginning of human flight, but it only received significant attention from the late 1970s [1]. Focus has been mainly placed on adverse effects of voluntary pilot action, the so-called Pilot-Induced Oscillations (PIO), which are caused by a mismatch between the actual vehicle dynamics and the mental model the pilot uses to anticipate the control action.

However, involuntary interactions may occur as well, often resulting in so-called Pilot-Augmented Oscillations (PAO). Those phenomena typically occur at frequencies that are too high to be effectively contrasted by the pilot's intentional action on the controls. The involuntary action is a direct consequence of the cockpit vibrations, which are filtered by the human limbs' biomechanics before being involuntarily fed into the control system.

Models of the voluntary pilot action for the investigation of piloted aircraft dynamics date back to the works of McRuer and Jex (see for example [2]), with the crossover model. Significant contributions came for example from the work of Hess with the structural pilot model [3], which takes the biomechanics into account in a simplified manner.

Several studies have investigated the effects of fixed-wing aircraft cockpit manipulators while performing compensatory tracking tasks (for example Magdaleno and McRuer [4] and McRuer and Magdaleno [5]). Subsequent work addressed the impact of vibration on pilot control, focusing on the feedthrough of vibration from the pilot to the control inceptors (for example Allen et al. [6], and Jex and Magdaleno [7]; see also the review by McLeod and Griffin [8], the work by Merhav and Idan [9] and the work of Höhne [10]). The effects of lateral stick characteristics on pilot dynamics were further investigated from flight data by Mitchell et al. [11].

Rotorcraft-Pilot Couplings (RPCs) did not receive as much attention in the open literature as their fixed-wing counterpart. This is especially true for involuntary couplings, despite the evidence of occurrences since the 1960s. In 1968 Gabel and Wilson [12] discussed the problem of external sling load instabilities, considering the case of vertical bounce of the sling load interacting with the pilot through the collective control system. In 1992, Prouty and Yackle [13] discuss RPC as a possible cause of an accident that occurred to the AH-56 Cheyenne during its troubled development. In 2007, Walden [14] presented an extensive discussion of aeromechanical instabilities that occurred with several rotorcraft during development and acceptance by the US Navy, including CH-46, UH-60, SH-60, CH-53, RAH-66, V-22 and AH-1. The history of tiltrotor development has seen several PAO events, from the early design and testing of the XV-15 technology demonstrator [15] to the aeroservoelastic pilot-in-the-loop couplings encountered during the development of the V-22 [16]. A complete database of PIO and PAO incidents occurred to fixed- and rotary-wing aircraft is reported in [1].

In the last decade, research efforts flourished in Europe; the coordinated activities of the GARTEUR HC AG-16 [17] and the ARISTOTEL 7th Framework Programme project [18,19] deserve a mention, along with other, independent activities (e.g. [20]).

The present work originates from the need to analyze the behavior of helicopters in interaction with the involuntary action of the pilot. Detailed multibody models of the vehicle and of the pilot's left arm have been developed for this purpose [21] using an original multi-

body dynamics formulation that is implemented in the free software MBDyn [22, 23], and used to numerically characterize the biodynamic feedthrough (BDFT) and neuromuscular admittance of the pilot [24].

The goal of this investigation is to simulate complex aeromechanical systems and their interaction with the human operator without the undue simplifications that are typically applied in pure flight mechanics analysis, like limiting the helicopter model to rigid blade dynamics and the pilot model to first- or second-order linear approximations of the biodynamics.

The innovative aspect of this work, to the authors' knowledge, is the use of a detailed biomechanical model of the pilot's arm that holds the collective control inceptor to actuate that control device. As a consequence, the voluntary action produced by the behavioral model with the aim of performing a tracking or regulatory task is naturally and intrinsically combined with the involuntary action that results from the environment, significantly from the vibrations of the cockpit. In previous work (e.g. [24]), the involuntary control inceptor rotation resulting from the biomechanical model of the pilot was added to the voluntary contribution before being fed to the control system actuators, bypassing the limbs' neuromuscular dynamics. Such approach is deemed insufficient because BDFT was experimentally [25, 26] as well as numerically [21, 24] observed to depend, among other parameters, on the reference position of the control inceptor, which may significantly change as a consequence of voluntary control action. The proposed model fills such gap, by ensuring consistency between control inputs and overall system configuration.

The work is organized as follows: in the first part, the structure of the piloted simulation problem is introduced; the biomechanical model originally presented in [21] is illustrated; the pilot's voluntary action model and its adaptation to time marching multibody analysis (direct integration of an initial value problem) are discussed, and simple applications of the isolated pilot model are presented. In the second part, the vehicle model and its integration with the pilot model are presented; the coupled model is used to analyze realistic problems.

The proposed approach is rather general, with respect to both pilot and vehicle modeling. Since the objective is the introduction of the voluntary action through the neuromuscular system, the analysis has been simplified by considering only the left arm holding the collective control inceptor, and limiting the overall motion of the vehicle to displacement along the vertical axis, focusing on a vertical maneuver in hover inspired by aircraft design standards.

It is worth noticing that often formulations and software implementations are specialized for given problem types. In the present case, a general-purpose formulation and implementation has been successfully used to model the details of both vehicle aeromechanics and pilot biomechanics, with few straightforward modifications, like user-defined constitutive laws for the muscles.

II. Pilot-Vehicle Modeling

The action of the pilot on the control inceptors originates from the combination of two logically distinct sources, shown in the block diagram of Fig 1, where $\Delta\theta$ is the control input (the collective control inceptor motion in the present context) and z is the motion of the vehicle (the heave motion in the present context), being z_d its desired value. One contribution

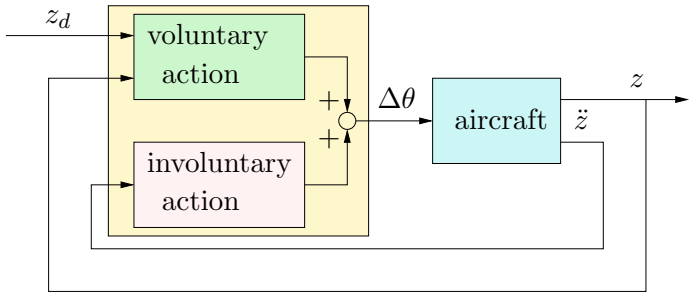

Figure 1. Abstract pilot model block diagram.

to $\Delta\theta$ is voluntary; in many cases it can be formulated as an attempt to perform a desired task by cancelling the error between a desired and an actual measure of the state of the vehicle, as perceived by the pilot through appropriate cues (cognitive input). The other contribution is involuntary; it is a consequence of the acceleration of the cockpit, which is fed through the pilot's body and filtered by the pilot's biodynamics (BDFT).

Both contributions, sent to the vehicle through a suitable control device (e.g. an inceptor), produce a response. Such response is further interpreted by the pilot to formulate the voluntary action and, at the same time, indirectly produces further involuntary action.

The scheme of Fig. 1 was used in [21, 24] to combine the voluntary contribution to the control input that is required to perform a maneuver with the involuntary one. In that model, the motion of the control inceptor caused by the involuntary action was added to a contribution originated by the cognitive action of the pilot. The mixing occurred downstream, as if the latter contribution came from an automatic flight control system.

In reality, however, the voluntary action originates at the pilot's cognitive level and is transformed into the corresponding motion of the control device by the pilot's neuromuscular system, through an appropriate muscular action. Figure 2 schematically illustrates how a neuromuscular model of the pilot action transforms a generic cue (e.g. a visual cue represented by the difference between the desired, z_d, and the actual position, z, as perceived by the pilot) into the muscle elongations, ℓ_{i_d}, and activations, a_i, that are required to compensate it.

The function of the block called 'neuromuscular model' can be split in a sequence of tasks:

- the motion $\Delta\eta$ required of the control inceptor to accomplish the desired task is de-

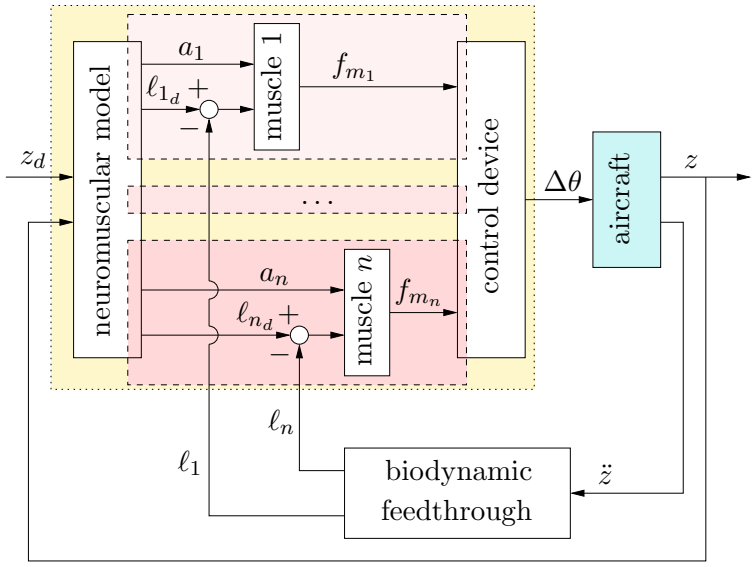

Figure 2. Neuromuscular pilot model block diagram.

termined, according to a 'mental' model of the vehicle dynamics that pilots typically acquire through training and experience;

- the limbs' motion required to produce the desired motion of the control inceptor is determined;
- the muscle action (the elongation ℓ_{i_d} and required force f_{m_i}, or better muscular activation a_i) needed to produce the motion of the limbs is determined.

Usually, biodynamic models of the pilot's limbs produce the actual muscle elongations, ℓ_i, as functions of cockpit motion, $\ddot{z}$, the so-called BDFT effect. The difference between the desired and the actual elongation of each muscle, and the corresponding activation, produce a change in the muscle force f_{m_i}. To this end, a muscle force model is needed. The Hill-like one proposed in [27] is used in the present work. The combination of synergistic and antagonistic muscle forces produces torques about the motor joints of the pilot's limbs and, in the end, about the hinge of the control device. As a consequence of such torque, the device rotates of an angle $\Delta\eta$, which is transformed by the control system (e.g. the control chain, which includes actuators in augmented controls aircraft, and may include an automatic flight control system) into the corresponding control input $\Delta\theta$ that is fed to the aircraft. The voluntary and involuntary feedback loops the pilot represents are closed by the resulting aircraft motion in terms of visual cues, exemplified and summarized in this work by the vertical position, z, and vibration, $\ddot{z}$.

A. Biomechanical Model of the Pilot

The biomechanical model of the pilot arm originally developed and presented in [21, 24] is briefly recalled in this section for completeness. The pilot's left arm is modeled using four rigid bodies that represent the humerus, the radius, the ulna, and the hand grasping the control inceptor. A sketch of the model is provided in Fig. 3.

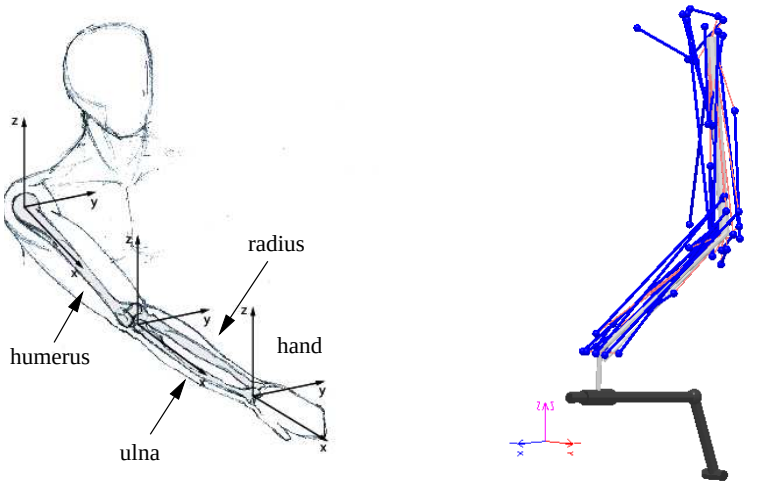

Figure 3. Multibody model of the arm holding the collective control inceptor.

The humerus is connected to the seat by a 'spherical' hinge to model a pilot tightly buckled by seat belts with shoulder harnesses. The ulna and the radius are connected to the humerus respectively by a 'revolute' and a 'spherical' joint to model the articulation of the elbow. An 'inline' joint prescribes that the distal ends of radius and ulna move along a line. The carpal complex connecting the hand to the radius is modeled by a 'universal' joint. The hand is rigidly connected to the control device, to simulate the firm grasp of the pilot (such assumption is a simplification that represents a limit case for a not easily quantifiable interaction; see for example [28], 13.4.1). The rigid bodies are connected by 25 muscle bundles (see Table 1 for details), modeled using deformable rod elements with a constitutive law discussed later. Data used in this work refer to a person of 70 kg body mass and 170 cm height (between 15% and 25% percentile for an adult male [29]). More details on the model, including dimensions, masses, and muscle properties can be found in [21, 24, 27, 30, 31].

Each rod defines a tension force between two points rigidly offset with respect to the bodies they connect. The force depends on the length and elongation rate of the rod. Specific constitutive properties have been developed, based on the simplified Hill-type muscle model proposed in [27].

Table 1. Arm muscles' properties: reference length (ℓ_0); max isometric force (f_{m0}); coordinates of insertion points 1 & 2 (x_1, y_1, z_1; x_2, y_2, z_2).

		ℓ_0 mm	f_{m0} N	x_1 mm	y_1 mm	z_1 mm	x_2 mm	y_2 mm	z_2 mm
Muscles connecting the humerus to the rest of the body									
1	Coracobrachialis	197	242.5	20	30	35	174	21	0
2	Deltoid — anterior fascicles	179	1142.6	35	25	35	136	-12	10
3	Deltoid — middle fascicles	159	1142.6	35	-22	20	136	-24	18
4	Deltoid — posterior fascicles	148	259.9	-35	10	0	136	-24	18
5	Latissimus dorsi	380	1059.2	-65	110	-290	75	25	9
6	Pectoralis major	147	1270.3	45	110	10	36	0	25
7	Supraspinatus	108	487.8	-36	80	35	-32	2	-13
8	Infraspinatus	111	1210.8	-32	80	-40	-26	0	-20
Muscles connecting the radius to the rest of the body									
9	Biceps brachii caput longus	388	624.3	0	-15	10	34	16	0
10	Biceps brachii caput brevis	324	435.6	20	30	25	3	16	0
Muscles connecting the ulna to the rest of the body									
11	Triceps brachii caput longus	290	798.5	-35	20	-20	-15	0	-22
Muscles connecting the humerus to the ulna									
12	Anconeus	55	350.0	300	-5	-12	-14	7	-11
13	Triceps brachii caput laterale/mediale	211	1248.6	112	0	-28	-27	0	-6
14	Brachialis	140	987.3	196	-8	16	17	15	5
Muscles connecting the humerus to the radius									
15	Brachioradialis	306	261.3	246	-7	0	238	-18	13
16	Pronator teres	148	566.2	270	33	-7	55	-18	12
Muscles connecting the humerus to the hand									
17	Flexor carpi ulnaris	317	128.9	265	27	-5	5	30	23
18	Extensor carpi ulnaris	290	93.2	269	-27	-5	5	30	-18
19	Extensor digitorum	387	100.7	269	-20	-20	8	0	-16
20	Flexor digitorum superficialis	380	226.6	275	27	-10	7	18	26
21	Flexor carpi radialis	307	74.0	275	27	-7	3	-20	32
22	Extensor carpi radialis	305	405.4	245	-20	0	5	-23	-11
Muscles connecting the ulna to the radius									
23	Pronator quadratus	33	75.5	200	7	14	236	27	23
24	Supinator	61	476.0	13	17	-8	28	13	-24
Muscle connecting the ulna to the hand									
25	Abductor pollicis longus	202	59.5	115	-21	-5	3	-18	23

According to [27], the force of the ith muscle is formulated as

$$f_{m_i} = f_{m0_i} \left(f_1(x_i) f_2(v_i) a_i + f_3(x_i) \right) \tag{1}$$

where $x_i = \ell_i / \ell_{0i}$ and $v_i = \dot{\ell}_i / V_{0i}$ are the non-dimensional muscle elongation and elongation rate, the former referred to a specific reference length of the muscle and the latter to a common conventional reference velocity [27]; a_i is the non-dimensional activation parameter, constrained by $0 \leq a_i \leq 1$.

The reference activation of the muscles is computed by solving the cascaded problem discussed in [21, 32]. An underdetermined inverse kineto-statics problem is solved first, to find the configuration of the limbs that complies with the boundary constraints and minimizes some ergonomy cost function (usually consisting in maximizing the distance from extreme joint positions). An inverse dynamics problem is then solved to find the joint torques that guarantee the equilibrium of the system. Since the inverse dynamics problem is overdetermined in terms of muscle forces, the force required of each muscle to provide the previously estimated joint torques is computed by minimizing the activation of the muscles, $\min_{a_i} \sum_i a_i^2$, constrained by $0 \leq a_i \leq 1$. As an example, the muscular activations required to hold the collective control inceptor at 10%, 50% and 90% are reported in Fig. 4. Some of the muscle bundles only activate for specific reference configurations; some do not activate at all, suggesting that in the given configuration they should push rather than pull to contribute to the required joint torques. However, all of them may be needed when reflexive activation and cognitive action are considered, as detailed later.

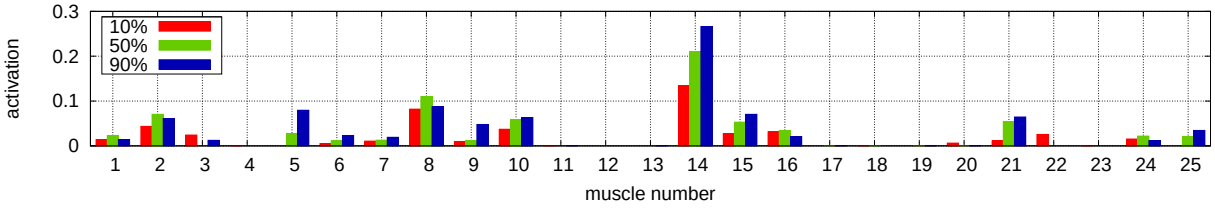

Figure 4. Muscular activation parameters for 10%, 50% and 90% collective control device reference position (muscles numbered according to Table 1).

As discussed in [21, 24], based on considerations made by Stroeve [33], a simple quasi-steady approximation of the reflexive contribution to the actuation based on the muscle length and elongation rate is considered,

$$a_i = a_{i_{\text{ref}}} - K_p \left(x_i - x_{i_{\text{ref}}} \right) - K_d v_i, \tag{2}$$

where, as discussed later, the reference length $x_{i_{\text{ref}}}$ is modified to produce the control inceptor motion requested by the voluntary pilot model. The use of a quasi-steady approximation

is justified by the consideration that the dynamics of muscular activation is characterized by relatively high frequencies (time constants between 10 and 40 ms, [34]) compared to the mechanical phenomena under consideration, which occur well below 10 Hz.

In [24], a relation between the approximate reflexive activation parameter K_p and the task a pilot is performing was established by comparing the results obtained from the numerical model and corresponding experimental results presented by Venrooij et al. in [35]. In that experiment, pilots were asked to perform a position task (PT), consisting in keeping the control inceptor in a prescribed position as accurately as possible, resisting forces; a relax task (RT), consisting in loosely keeping the control inceptor about a prescribed position; a force task (FT), consisting in yielding to forces without trying to keep the inceptor in a specific position.

Each task required human operators to attain different levels and combinations of muscular activation. The PT requires a significant amount of reflexive activation in addition to the reference amount required to counteract the own weight of the arm, whereas the other tasks require a much lower level of reflexive activation. High reflexive activation can be intuitively associated with pilot's reactivity and promptness in responding to perturbations and external stimuli in general. BDFT appears to be most prone to causing RPCs when the reflexive muscular activation related to PT is considered [24, 36]. Indeed, it has been assessed that reflexive activation parameters associated with less aggressive pilot behavior (e.g. RT) lead to less prompt and slightly more damped response. For this reason, only the parameters related to PT are used in the coupled pilot-vehicle analyses presented in this work.

In [25], Mayo reported significant dependence of BDFT gain on collective inceptor reference position; no attempt was made at transfer function identification parametrized in the inceptor position. In [26], Masarati et al. presented experimental BDFT frequency responses and reported significant dependence of gain and poles of identified pilots' BDFT transfer functions on collective inceptor reference position. Specifically, the frequency and the damping factor reduced when the collective was increased. In [24], Masarati and Quaranta, using the same biomechanical model discussed in the present work, obtained numerical trends in BDFT that were consistent with those of [26], and were subsequently extended in [37] by Zanlucchi et al. These considerations support the opportunity to preserve consistency between the control input and the actual position of the control inceptor.

B. Cognitive Pilot Model

According to the block diagram of Fig. 5, the voluntary control of the pilot is

$$\Delta\theta = H_{\theta e_z}(s)\,(z_d - z) + H_{\mathrm{ff}}(s) z_d. \tag{3}$$

The function $H_{\theta e_z}(s)$ encompasses the strategy elaborated by the pilot acting as a regulator to cancel the error $e_z = z_d - z$ between the desired, z_d, and the actual position, z. The function $H_{\text{ff}}(s) \approx \hat{H}_{z\theta}^{-1}(s)$ represents a feedforward contribution based on an approximated inverse model of the vehicle's response to the controls, low-pass filtered to only account for the vehicle behavior in the pilot's bandwidth. Both functions express the mental model of the vehicle the pilot's control action is based on.

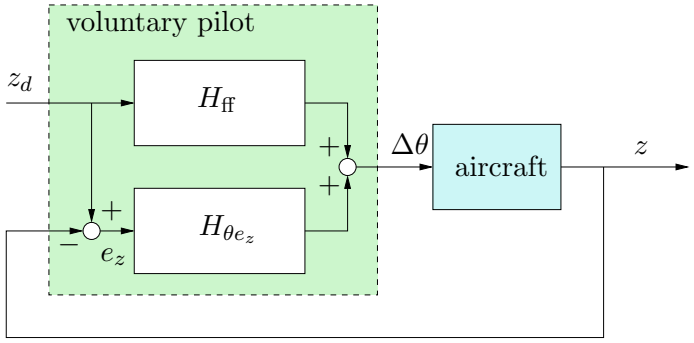

Figure 5. Voluntary pilot model block diagram.

For the vertical axis in hover, the simplest model within the pilot's bandwidth that can be obtained from the linearization of the equilibrium equation along the vertical axis is

$$M\ddot{z} = Z_{/\dot{z}}\dot{z} + Z_{/\theta}\Delta\theta, \tag{4}$$

where M is the mass of the helicopter and Z is the net vertical force component, i.e. thrust minus weight, with $Z_{/\theta} > 0$ (thrust changes according to the collective control) and $Z_{/\dot{z}} < 0$ (velocity perturbations cause opposite thrust perturbations). The approximate transfer function is

$$\hat{H}_{z\theta}(s) = \frac{Z_{/\theta}/M}{s(s - Z_{/\dot{z}}/M)}, \tag{5}$$

where Z/M is the net specific force perturbation (dimensionally an acceleration). The inverse of Eq. (5) must be low-pass filtered by a filter at least of the third order to obtain a strictly proper function [38]. Some simple anti-windup strategy has been considered to limit the phenomenon when tracking a rapidly changing desired position, by saturating the accumulated integral of the error. These aspects are not described in detail as they are considered inessential with respect to the main topic of the work.

In the present work, two simple voluntary pilot feedback functions have been initially considered. The first one is based on McRuer's crossover model [2]. The model results from the observation that for a broad variety of simple tasks the loop transfer function $H_L(s) = H_{z\theta}(s)H_{\theta e_z}(s)$ can be approximated by an integrator and a time delay in the

vicinity of the crossover frequency of the function, ω_c, namely

$$H_L(s) = H_{z\theta}(s)H_{\theta e_z}(s) = \frac{\omega_c}{s}\mathrm{e}^{-s\tau_e}. \tag{6}$$

According to this model, and considering the approximated vehicle transfer function $\hat{H}_{z\theta}(s)$ of Eq. (5) under the assumption that it captures the behavior of the vehicle in the vicinity of the crossover frequency, the pilot feedback function is

$$H_{\theta e_z}(s) \approx \hat{H}_{z\theta}^{-1}(s)\frac{\omega_c}{s}\mathrm{e}^{-s\tau_e} = \frac{s - Z_{\dot{z}}/M}{Z_{/\theta}/M}\omega_c\mathrm{e}^{-s\tau_e}. \tag{7}$$

To be usable in a time marching simulation, such model needs to be made strictly proper by adding a low-pass filter at least of second order, which is characterized by two poles,

$$H_{\theta e_{\text{filtered}}}(s) = \frac{\alpha_2}{s^2 + \alpha_1 s + \alpha_2}\frac{s - Z_{\dot{z}}/M}{Z_{/\theta}/M}\omega_c\mathrm{e}^{-s\tau_e} \tag{8}$$

that for $0 < \alpha_1 \leq 2\sqrt{\alpha_2}$ (i.e. when they are complex conjugated) produce a cut frequency $\sqrt{\alpha_2}$ slightly higher than ω_c.

The second voluntary pilot feedback function is the one derived from the work of Szabolcsi [39] and used in [40],

$$H_{\theta e_z}(s) = K_A\frac{(T_3 s + 1)}{(T_1 s + 1)(T_2 s + 1)}\mathrm{e}^{-s\tau_e}. \tag{9}$$

According to [40], the parameters of the model are:

- K_A: the pilot's gain;
- T_1: the lag time constant, describing "the ease with which the pilot generates the required input";
- T_2: the neuromuscular lag time constant;
- T_3: the lead time constant, which represents the ability of the pilot in predicting the behavior of the vehicle within the pilot's bandwidth;
- τ_e: a time delay that represents the time that lapses between the sensing of a cue and the voluntary reaction of the pilot.

Note that Eq. (9) of the second model has the same structure of Eq. (8) of the first one, with $K_A = -\omega_c Z_{\dot{z}}/Z_\theta$, $T_3 = -M/Z_{\dot{z}}$, and $T_1 + T_2 = 1/\alpha_2$, $T_1 T_2 = \alpha_1/\alpha_2$. In practice, the model of Eq. (9) gives a specific physical meaning to the poles of the low-pass filter, purposely

introduced in Eq. (8) to make it suitable for time marching analysis, which are assumed to be real rather than complex conjugated.

The pole characterized by T_2 in the model of Eq. (9) plays the role (and is a gross approximation) of the low-pass filtering effect of the pilot limbs' biomechanics (it is worth noticing that in the original work of Szabolcsi [39], an alternative second-order approximation was proposed using two complex-conjugate poles; a similar approach was proposed by Hess in his fundamental work on the structural pilot model [3]). Clearly, in the present work such role is played by the detailed biomechanical model of the pilot.

For both models, the time delay has been approximated using a second-order Padé form,

$$\mathrm{e}^{-s\tau_e} \cong \frac{1 - \frac{\tau_e}{2}s + \frac{\tau_e^2}{12}s^2}{1 + \frac{\tau_e}{2}s + \frac{\tau_e^2}{12}s^2}, \tag{10}$$

and the whole transfer function has been transformed in the time domain in form of a linear, time invariant state-space system that produces the desired intentional control inceptor rotation as a function of the altitude error. Given the clear similarity between the two models, only results obtained with the crossover model are presented in the following.

More sophisticated voluntary pilot models can be used, for example when specific tasks need to be addressed (e.g. models derived from Gray's work on Boundary Avoidance Task (BAT) [41–43]). The previously discussed simple models are preferred in this context since the focus is on producing the effect of the pilot's intentional behavior throughout the same detailed biomechanical model that is used to simulate the involuntary behavior. However, the opportunity to take into account a voluntary change in control strategy and/or an involuntary change in biodynamic properties of the limbs triggered by a change in control demand of the task will be investigated in the future as a potential source of RPC.

C. Pilot Voluntary Action Through the Biomechanical Model

The voluntary action of the pilot defined by Eq. (3) in terms of blade collective pitch as a function of the desired and actual state of the vehicle must be transformed into appropriate commands to the muscles by means of a neuromuscular model.

Consider a linear map between the collective control perturbation, $\Delta\eta$, and the muscle elongation perturbations, $\Delta\boldsymbol{\ell}$,

$$\Delta\boldsymbol{\ell} = \boldsymbol{\ell}_{/\eta}\Delta\eta \tag{11}$$

In the simplest case, a (linear) mapping can be defined between the rotation of the collective

control inceptor, η (the control throw), and the static blade collective pitch rotation, θ, namely

$$\Delta\theta = G_c \Delta\eta \tag{12}$$

(in the case at hand, $G_c \approx 0.5$ radian/radian, since a typical control inceptor end to end rotation is about 35 deg, whereas the blade collective pitch range is between 16 and 20 deg).

A more realistic model also considers the dynamics of the control system actuators. In this work, they are approximated using either first- or second-order low-pass filters, e.g.

$$\Delta\theta = G_c \frac{1}{1+ps} \Delta\eta \tag{13}$$

with a time constant p of about 0.012 s, or

$$\Delta\theta = G_c \frac{1}{1 + 2\xi_a s/\omega_a + (s/\omega_a)^2} \Delta\eta, \tag{14}$$

with a cut frequency ω_a of about 12 Hz and a damping factor ξ_a of about 0.4.

In advanced rotorcraft, a sophisticated flight control system (FCS) may further modify the pilot controls prior to feeding them to the actual pitch control mechanism. Although the details of such systems are beyond the scope of the current work, a net effect they could have on the pilot's commanded control is a further delay of up to 100 ms caused by the digital filtering and processing of the control inceptor motion [1,44]. Such delay may play a critical role in reducing the phase margin of the closed loop system.

The blade collective pitch demand can be mapped onto the corresponding muscle elongation perturbation demand,

$$\Delta\boldsymbol{\ell} = \boldsymbol{\ell}_{/\eta} \frac{1}{G_c} \left(\left(H_{\theta e_z}(s) + \hat{H}_{z\theta}^{-1}(s) \right) z_d - H_{\theta e_z}(s)\, z \right) \tag{15}$$

The actual muscle elongation demand is filtered by a low-pass filter that includes an electromechanical delay of about 50 ms, $H_{\mathrm{NMD}}(s)$ (values between 10 and 120 ms are reported in the literature, see for example [45]).

The filtered muscle elongation demand is added to the reference muscle elongation used in the quasi-steady approximation of the reflexive activation of Eq. (2), which becomes

$$a_i = a_{i_{\mathrm{ref}}} - K_p \left(x_i - x_{i_{\mathrm{ref}}} - H_{\mathrm{NMD}}(s) \Delta x_{i_{\mathrm{ref}}} \right) - K_d v_i. \tag{16}$$

The modified reference length is used to produce the control inceptor motion requested by the voluntary pilot model.

Rather than resorting to a complex inverse model of the pilot biomechanics, given the simplicity of the specific problem, a numerical linearization has been considered. The approach used in this work assumes that only small perturbations of the limbs' motion about a steady reference configuration are required, involving limited amount of muscular activation.

The value of $\boldsymbol{\ell}_{/\eta}$ is computed according to the procedure:

- prescribe a small rotation $\Delta\eta$ to the control inceptor;
- measure the length change of each muscle, $\Delta\ell_i$;
- measure the activation change of each muscle, Δa_i.

The force change in each muscle is

$$\Delta f_{m_i} = f_{m0_i} \left(f_1(x_{i_{\text{ref}}} + \Delta x_i)(a_{i_{\text{ref}}} - K_p \Delta x_i) + f_3(x_{i_{\text{ref}}} + \Delta x_i) - f_1(x_{i_{\text{ref}}}) a_{i_{\text{ref}}} - f_3(x_{i_{\text{ref}}}) \right), \tag{17}$$

considering that in isometric conditions $v_i = 0$ and $f_2(0) \equiv 1$. Assuming the elongation change Δx_i is small enough that a local linearization of $f_1(x)$, $f_3(x)$ is an acceptable approximation, the force perturbation becomes

$$\Delta f_{m_i} = f_{m0_i} \left((f_{1/x} a_{i_{\text{ref}}} + f_{3/x} - f_1(x_{i_{\text{ref}}}) K_p) \Delta x_i - f_{1/x} K_p \Delta x_i^2 \right) \tag{18}$$

Consider now a change of reference length such that $\Delta\ell_{i_{\text{ref}}} \equiv \Delta\ell_i$, thus $\Delta a_i = \Delta a_{i_{\text{ref}}}$, since the reflexive change of activation is zero. Then, the change of muscle force is

$$\Delta \tilde{f}_{m_i} = f_{m0_i} \left((f_{1/x} a_{i_{\text{ref}}} + f_{3/x}) \Delta x_i + (f_1(x_{i_{\text{ref}}}) + f_{1/x} \Delta x_i) \Delta a_{i_{\text{ref}}} \right) \tag{19}$$

If the change of reference length (and of reference activation) is applied to an otherwise unloaded arm, assuming that the change of configuration is small enough, no first-order change of muscular force is needed. As a consequence, $\Delta \tilde{f}_{m_i} \cong 0$, which requires a change of reference activation

$$\Delta a_{i_{\text{ref}}} \cong -\frac{f_{1/x} a_{i_{\text{ref}}} + f_{3/x}}{f_1(x_{i_{\text{ref}}} + \Delta x_i)} \Delta x_i. \tag{20}$$

This implies that when the simple reflexive model of Eq. (2) is considered for the muscular activation, to prescribe a rotation of the control inceptor both the desired reference length of the muscles, $\Delta\ell_{i_{\text{ref}}}$, and the corresponding reference activation, $\Delta a_{i_{\text{ref}}}$, must be modified accordingly.

D. Basic Voluntary/Involuntary Pilot-Control Device Interaction Results

BDFT has been estimated using system identification from detailed multibody simulation. According to functions proposed in the literature, either identified from experiments [25, 26] or from numerical models [24], the BDFT between the collective control inceptor motion and the acceleration of the cockpit can be represented by a second-order low-pass filter,

$$H_{\eta\ddot{z}}(s) = \frac{b_0\omega_p^2}{s^2 + 2\xi_p\omega_p s + \omega_p^2}. \tag{21}$$

In the case of the 'position task' (PT) pilot, with the collective control inceptor held about the 50% position, the function (shown in Fig. 6) is characterized by a natural frequency $\omega_p = 16.7$ radian/s (2.66 Hz), a damping factor $\xi_p = 0.251$, and a static gain $b_0 = 1.47$ radian/m.

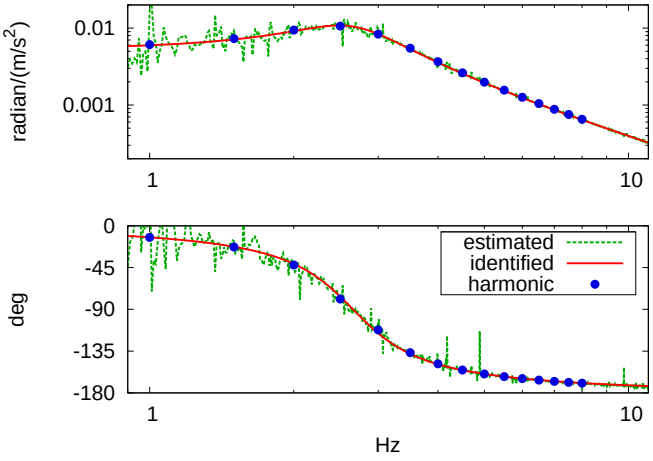

Figure 6. Biodynamic feedthrough: transfer functions 'estimated', 'identified' and obtained using 'harmonic' excitation.

Data have been obtained by applying a random vertical acceleration, band-pass filtered in the 1–10 Hz range, to the multibody model of the pilot's arm. The transfer function estimated from the input and the resulting collective control inceptor rotation is labeled 'estimated'. The corresponding identified transfer function is labeled 'identified'; the formula is that of Eq. (21). The analogous function obtained from the response to limited amplitude harmonic excitation is labeled 'harmonic'.

The subsequent applications verify how the actual rotation of the control inceptor, sketched in Fig. 7, resembles the demanded one.

The result is shown in Figs. 8 and 9. Figure 8 shows the actual motion when a large step input (6 deg) is demanded. Figure 9 shows the actual motion when the the collective control inceptor rotation measured during flight simulator tests originally presented in [46] is demanded. The neuromuscular model is able to accurately track the motion demand, with

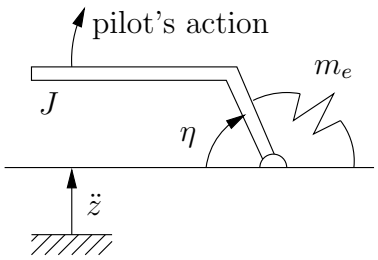

Figure 7. Sketch of collective control device.

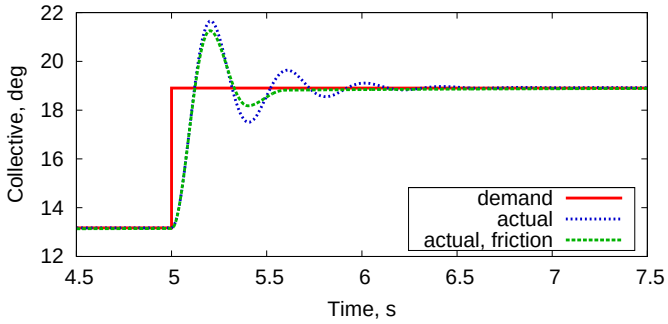

Figure 8. Step input: collective control inceptor demanded and actual rotation.

minimal delay and small, damped oscillations occurring when the input variation is excessively abrupt. In Fig. 8, the curve obtained with a 'loose' inceptor, i.e. without any reaction moment, is labeled 'actual'. Additionally, the curve labeled 'actual, friction' illustrates the response obtained also considering a moment of the form

$$m_e = -C_1 \tanh(C_2 \dot{\eta}), \tag{22}$$

that contrasts the rotation of the control inceptor, emulating the friction that often characterizes the collective control inceptor, with $C_1 = 0.3$ N·m and $C_2 = 300$ s/radian.

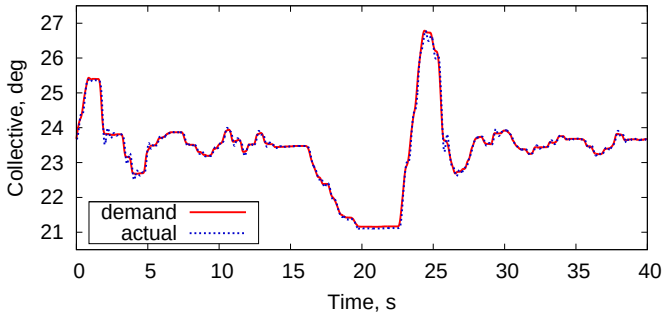

Figure 9. Input from measured data: collective control inceptor demanded and actual rotation.

III. Analysis of Piloted Vehicle Model

This section presents the analysis of a detailed multibody model of a vehicle controlled by the previously described pilot model. Both models are developed within the same multibody analysis following a monolithic approach.

A. Aeromechanical Model of the Vehicle

A multibody model of a generic medium weight helicopter, with articulated main rotor, has been developed using the free general-purpose multibody solver MBDyn [23]. The aeromechanical data of the helicopter is loosely related to that of the Sud Aviation (now Airbus Helicopters) SA330 Puma. The multibody model has been presented first in [47], where it was correlated to an independently developed model based on the same data, and on limited experimental data. The same model was used in [24], where the involuntary biomechanics of the pilot was used to analyze the effect of BDFT.

The choice of this specific helicopter was dictated by the broad availability of aeroelastic data in the open literature. The aeromechanical model is briefly described in the following for completeness, and to give the reader an indication of its complexity and detail.

The aspects of the vehicle that according to [48] are essential for aeroelastic RPCs have been considered. The main rotor aeroelasticity is modeled in detail. The structural dynamics of the 4 rotor blades are described using the original Geometrically Exact Beam Formulation (GEBF) presented in [49]. Each blade is modeled using five three-node beam elements.

Figure 10 shows a detail of the rotor hub. The root of each blade is connected to the hub by a sequence of 'revolute' hinges that reproduce the exact kinematics of the lag and flap hinges and of the pitch bearing. A rigid body that can lag (i.e. rotate about an axis that is parallel to the rotation axis of the rotor) is connected to the rotor hub for each blade. A linear viscous element models the viscous damper that acts between the lagging body and the hub. Another 'revolute' hinge models the connection between the rigid body that can flap (i.e. rotate about an axis that is orthogonal to both the blade and the rotation axes) and the lagging body of each blade. The root of the blade is connected to the flapping body by a third 'revolute' hinge that models the bearing that allows the pitching of the blade. The root of the blade, right after the pitch bearing, is also connected to the rotating swashplate by a pitch link, namely an elastic rod loosely directed along the rotation axis of the rotor and offset from the blade axis, that transmits the pitch control to the blade, also accounting for the mechanical compliance of the pitch control mechanism.

The main rotor is connected to a Component Mode Synthesis (CMS) model of the airframe by a joint that prescribes the angular velocity of the hub. The fixed part of the swashplate, including the linear actuators that command its position and orientation, is also

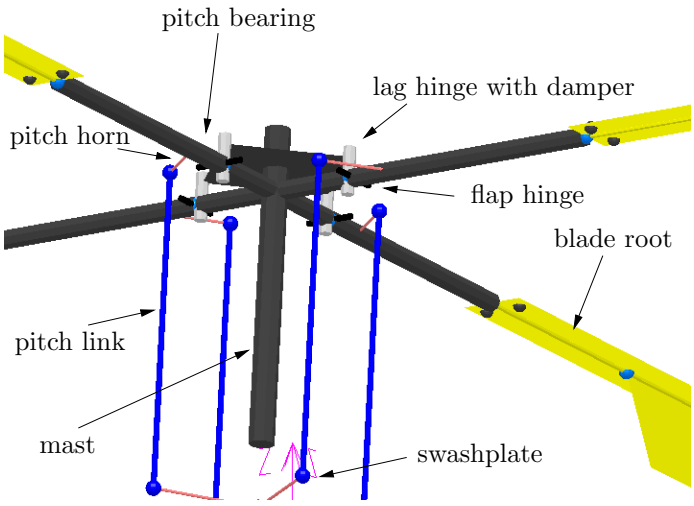

Figure 10. Detailed view of the main rotor hub.

connected to the airframe model. The airframe model is made of a rigid body that accounts for the rigid body dynamics of the vehicle, and up to 8 Normal Vibration Modes (NVM).

The motion of selected points, namely the connections with the main and tail rotors, and the locations of the pilot and co-pilot seats, is described in terms of their location in the reference model and their participation to those NVM. The NVM in the band of frequencies of interest (up to about 30 Hz) and with appreciable modal participation of the main rotor and crew seats have been chosen. The frequency of the lowest structural mode is about 6.8 Hz; the first mode with significant airframe bending in the vertical direction is at about 8.0 Hz.

The airframe dynamics are completed by simple lookup-table aerodynamics of the tail surfaces. The tail rotor aeromechanics is approximated by a lumped lateral force whose magnitude depends on the related collective pitch control and on the normal component of the velocity at the center of the rotor.

B. Results of the Coupled System Analysis

The proposed model of the joint voluntary and involuntary pilot action has been integrated in the coupled helicopter-pilot model, as shown in Fig. 11. The airframe is modeled using normal vibration modes. only the location and the modal displacement of selected nodes (pilots' seats, main and tail rotor attachments, aircraft center of mass) were available[a]. The shoulder and the collective control inceptor are hinged to the seat node respectively by a

[a]Representative airframe data was only available through private communications; as such, they are not reported in detail. It is understood that the exact values are not critical for the relevant aspects of the analysis.

'spherical' and a 'revolute' hinge; the corresponding muscle bundles are connected to the seat node accordingly. The rotation of the collective control inceptor is logically fed into the swashplate actuators as actuator displacement demand.

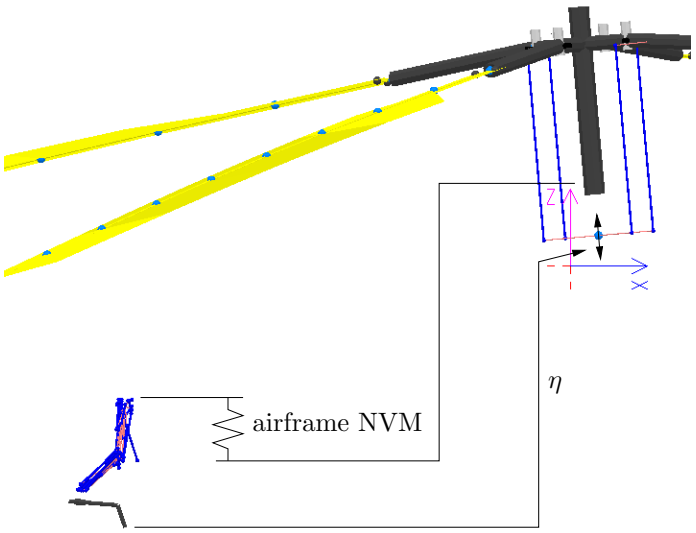

Figure 11. Multibody model of main rotor and pilot.

In the present analysis, the rigid-body motion of the helicopter is only allowed along and about the vertical axis. Such restriction has been introduced because only the left arm is modeled, the one that commands the collective control inceptor and thus directly determines the vertical thrust produced by the rotor.

The intentional action of the pilot has been modeled using McRuer's crossover model. The parameters of what corresponds to the pilot's mental model of the helicopter are listed in Table 2 (adapted from [50] with reference to the IAR330, a 'heavy' version of the SA330), along with those of the pilot (from [2]) and of the low-pass filter, a second-order low-pass Butterworth filter with the cut frequency set to 3.1 radian/s.

Table 2. Parameters of the voluntary pilot model.

M	7345.0	kg
$Z_{/\dot{z}}/M$	-0.8	s^{-1}
$Z_{/\theta}/M$	113.0	$\mathrm{m{\cdot}s^{-2}{\cdot}radian^{-1}}$
ω_c	1.0	$\mathrm{radian{\cdot}s^{-1}}$
τ_e	0.38	s
$\omega_f = \sqrt{\alpha_2}$	3.10	$\mathrm{radian{\cdot}s^{-1}}$
$\xi_f = \alpha_1/(2\omega_f)$	$1/\sqrt{2}$	n.d.

Figure 12 presents the results of the simulation of a task inspired by the vertical maneuver specified in the United States rotorcraft handling qualities performance design specification,

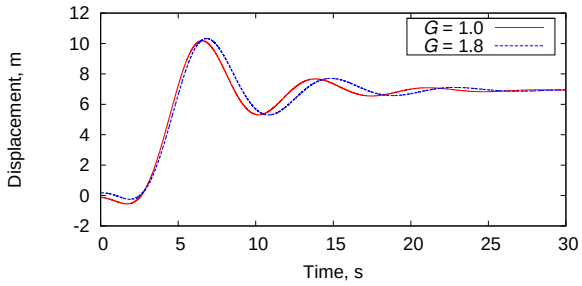

(a) Helicopter vertical displacement.

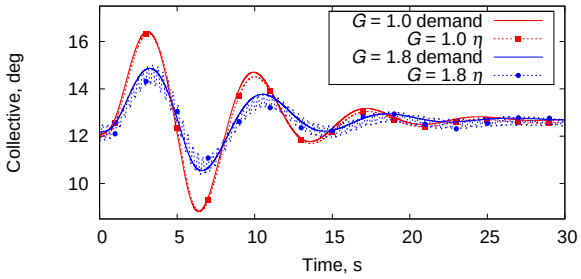

(b) Collective stick motion.

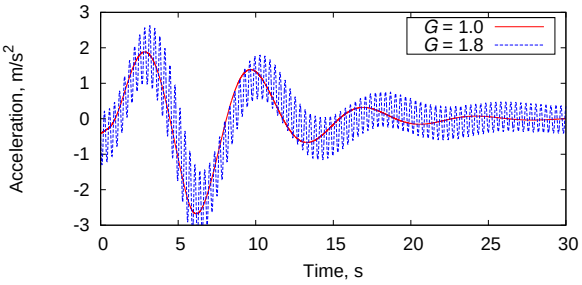

(c) Helicopter vertical acceleration.

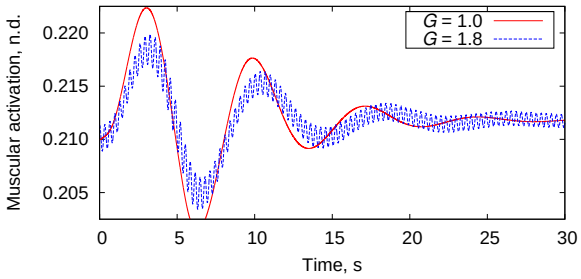

(d) Brachialis muscle activation.

Figure 12. Helicopter vertical maneuver, 'loose' control inceptor.

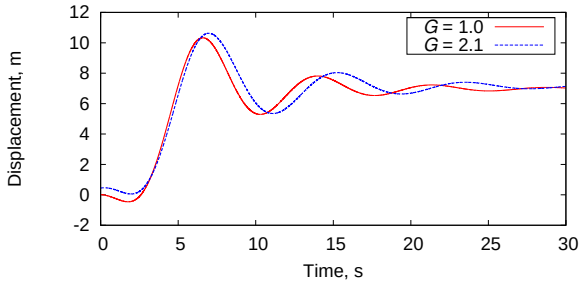

(a) Helicopter vertical displacement.

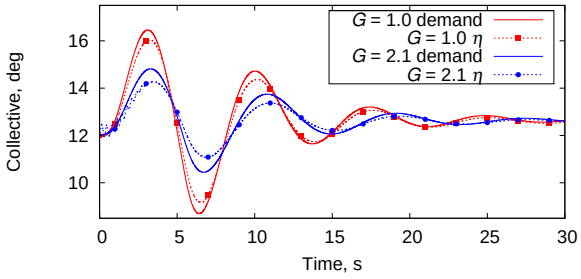

(b) Collective stick motion.

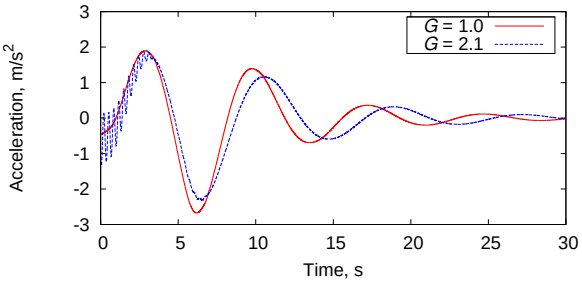

(c) Helicopter vertical acceleration.

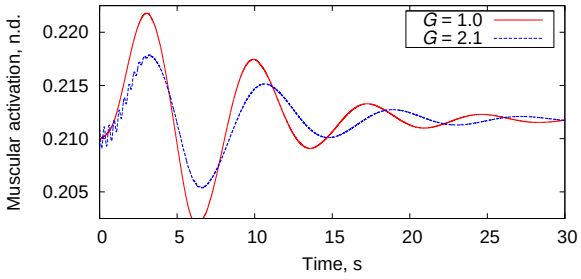

(d) Brachialis muscle activation.

Figure 13. Helicopter vertical maneuver, control inceptor with emulated friction.

ADS-33E-PRF [51]. During the maneuver, the pilot changes the altitude of the helicopter by 25 ft (about 8 m) starting and ending in hover condition, to rapidly unmask an attack/scout helicopter or to assess the heave axis controllability of a utility/cargo helicopter with precision station keeping. Since the specification only prescribes the purpose of the maneuver, the desired trajectory of the aircraft is arbitrarily chosen as a vertical motion $z_d = (1 - \cos(\pi t/T))A/2$ with $T = 5$ s and $A = 25$ ft, for $0 \leq t \leq T$.

In the following, the gearing ratio is modified to act as a sort of a physical "feedback gain". Rather than changing G_c, an amplification factor G is considered, such that $\Delta\theta = GG_c\Delta\eta$, with $G = 1$ corresponding to nominal gearing ratio. Figure 12(a) compares the vertical displacement of the helicopter with nominal and nearly doubled gearing ratio ($G = 1.8$); the latter makes the coupled vehicle-pilot system barely stable. Figure 12(c) shows the vertical acceleration of the helicopter. Figure 12(b) shows the collective control inceptor rotation demand and the actual rotation after the action of the biomechanical model. Note that when the gearing ratio is increased from 1.0 to 1.8, the inceptor rotation demand reduces by a factor $1/G = 5/9$, since the maneuver requires the same amount of blade pitch rotation, which is obtained with a smaller rotation of the control inceptor. Figure 12(d) shows the muscular activation of the 'brachialis' muscle (which is significantly involved in the flexure of the elbow, see Table 1). The brachialis muscle shows the largest activation level for this specific maneuver.

Figure 13 is similar to Fig. 12; only, in this case the control inceptor is not loose. On the contrary, friction is emulated according to Eq. (22), with $C_1 = 0.3$ N·m and $C_2 = 300$ s/radian. The trends are quite similar. The main difference, when $G = 1.0$, is that the presence of emulated friction increases the difference between the demanded and the actual control inceptor rotation (Fig. 13(b) vs. Fig. 12(b)). Another important difference is that with emulated friction the coupled pilot-vehicle system remains stable at a value of G about 15% higher than in case of loose control.

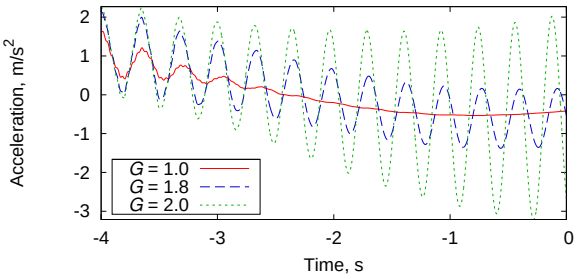

Figure 14. Helicopter vertical acceleration after impulsive perturbation, 'loose' control inceptor.

Figure 14 shows the vertical acceleration of the helicopter during a short transient before the maneuver is initiated, after the system has been perturbed impulsively. The figure shows

that for nominal gear ratio ($G = 1.0$) the oscillations associated with the interaction between the main rotor coning mode (a major playing factor in collective bounce, as pointed out in [52]) and the pilot biodynamics quickly vanish. For $G = 1.8$ the oscillations persist, whereas for $G = 2.0$ they diverge. Moreover, the frequency of the oscillations slightly increases with G, from about 2.9 Hz with 10% damping for $G = 1.0$ to about 3.1 Hz and slightly negative damping for $G = 2.0$. Such increase is mainly a consequence of the fact that the coupling of the pilot's limb biomechanics (whose pole is at about 2.6 Hz) with the main rotor coning aeromechanics (at about 4 Hz) increases with G.

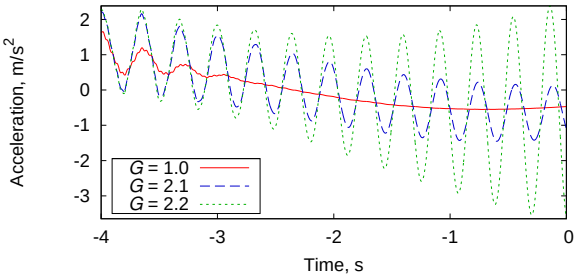

Figure 15. Helicopter vertical acceleration after impulsive perturbation, control inceptor with emulated friction.

Figure 15 is analogous to Fig. 14, with emulated friction instead of the loose control inceptor. It shows that the presence of friction makes the coupled system stable for larger values of G (about 15% larger). Also, for G set to the nominal value of 1.0, the initial oscillations triggered by the impulsive perturbations vanish more quickly.

This section showed how the introduction of the pilot's voluntary action by means of the biomechanical model of the arm preserves consistency between the position of the inceptor, which determines the input of the control system, and the biodynamic feedthrough characteristics of the pilot. As discussed previously, there is indirect numerical and experimental evidence that such consistency can play a role in determining the actual BDFT. Further investigation is needed to determine its importance, with the ultimate goal of contributing to practical procedures to define pilot BDFT envelopes, boundaries, and most critical operating conditions, to support the development of rotorcraft that are RPC-free by design.

Thorough validation of the biomechanical model is needed, to improve its reliability in predicting biodynamic feedthrough. Other directions for improvement encompass statistical considerations on inter-subject (e.g. height, weight), as well as intra-subject (reflexive activation, control inceptor configuration) variability of biomechanical properties. Finally, the same analysis should be formulated for the right arm holding the cyclic control inceptor.

IV. Conclusions

This work presented the analysis of the pilot interaction with the aeromechanics of a helicopter in relation with hover and precision repositioning maneuvers along the vertical axis. The voluntary action of the pilot that determines the collective pitch control is formulated using McRuer's crossover model, a simple behavioral model that characterizes the control of simple tasks by human subjects. Such action is transformed into the actuation of the collective control inceptor by prescribing the corresponding desired muscle elongation in a detailed biomechanical model of the pilot's left arm. The desired elongation of each muscle is tracked using a quasi-steady approximation of the muscular activation that simulates response to reflexive stimuli. The coupled pilot-vehicle model is formulated and applied to the simulation of standard maneuvers. The results showed that the proposed biomechanical model can be successfully used to transform the voluntary action of the pilot in realistic motion of the control inceptors. As a consequence, when that signal is used as input of the control system, consistency is preserved between the control input and the configuration of the pilot's arm, providing consistent feedthrough of cockpit vibrations to the control system.

Acknowledgments

The authors gratefully acknowledge the contributions of Vincenzo Muscarello (helicopter modeling) and Andrea Zanoni (development of the pilot's biomechanical model). The first two authors have received funding for the research leading to these results from the European Community's Seventh Framework Programme (FP7/2007–2013) under grant agreement N. 266073.

References

[1] Pavel, M. D., Jump, M., Dang-Vu, B., Masarati, P., Gennaretti, M., Ionita, A., Zaichik, L., Smaili, H., Quaranta, G., Yilmaz, D., Jones, M., Serafini, J., and Malecki, J., "Adverse rotorcraft pilot couplings — Past, present and future challenges," Progress in Aerospace Sciences, Vol. 62, October 2013, pp. 1–51, doi:10.1016/j.paerosci.2013.04.003.

[2] McRuer, D. T. and Jex, H. R., "A Review of Quasi-Linear Pilot Models," Human Factors in Electronics, IEEE Transactions on, Vol. HFE-8, No. 3, September 1967, pp. 231–249, doi:10.1109/THFE.1967.234304.

[3] Hess, R. A., "Theory for Aircraft Handling Qualities Based Upon a Structural Pilot Model," J. of Guidance, Control, and Dynamics, Vol. 12, No. 6, 1989, pp. 792–797, doi:10.2514/3.20483.

[4] Magdaleno, R. E. and McRuer, D. T., "Effects of Manipulator Restraints on Human Operator

Performance," AFFDL TR-66-72, 1966.

[5] McRuer, D. T. and Magdaleno, R. E., "Human Pilot Dynamics with Various Manipulators," AFFDL-TR 66-138, 1966.

[6] Allen, R. W., Jex, H. R., and Magdaleno, R. E., "Manual Control Performance and Dynamic Response During Sinusoidal Vibration," AMRL-TR 73-78, October 1973.

[7] Jex, H. R. and Magdaleno, R. E., "Biomechanical models for vibration feedthrough to hands and head for a semisupine pilot," Aviation, Space, and Environmental Medicine, Vol. 49, No. 1–2, 1978, pp. 304–316.

[8] McLeod, R. W. and Griffin, M. J., "Review of the effects of translational whole-body vibration on continuous manual control performance," Journal of Sound and Vibration, Vol. 133, No. 1, 1989, pp. 55–115, doi:10.1016/0022-460X(89)90985-1.

[9] Merhav, S. J. and Idan, M., "Effects of biodynamic coupling on the human operator model," J. of Guidance, Control, and Dynamics, Vol. 13, No. 4, 1990, pp. 630–637, doi:10.2514/3.25380.

[10] Höhne, G., "Computer aided development of biomechanical pilot models," Aerospace Science and Technology, Vol. 4, No. 1, January 2000, pp. 57–69, doi:10.1016/S1270-9638(00)00117-6.

[11] Mitchell, D. G., Aponso, B. L., and Klyde, D. H., "Effects of cockpit lateral stick characteristics on handling qualities and pilot dynamics," CR 4443, NASA, 1992.

[12] Gabel, R. and Wilson, G. J., "Test Approaches to External Sling Load Instabilities," Journal of the American Helicopter Society, Vol. 13, No. 3, 1968, pp. 44–55, doi:10.4050/JAHS.13.44.

[13] Prouty, R. W. and Yackle, A. R., "The Lockheed AH-56 Cheyenne — Lessons learned," AIAA Aircraft Design Systems Meeting, Hilton Head, SC, USA, August 24–26 1992, AIAA-1992-4278.

[14] Walden, R. B., "A Retrospective Survey of Pilot-Structural Coupling Instabilities in Naval Rotorcraft," American Helicopter Society 63rd Annual Forum, Virginia Beach, VA, May 1–3 2007, pp. 1783–1800.

[15] Bilger, J., Marr, R., and Zahedi, A., "Results of Structural Dynamic Testing of the XV-15 Tilt Rotor Research Aircraft," Journal of the American Helicopter Society, Vol. 27, No. 2, 1982, pp. 58–65.

[16] Parham, Jr., T., Popelka, D., Miller, D. G., and Froebel, A. T., "V-22 Pilot-in-the-loop Aeroelastic Stability Analysis," American Helicopter Society 47th Annual Forum, Phoenix, Arizona (USA), May 6–8 1991.

[17] Dieterich, O., Götz, J., DangVu, B., Haverdings, H., Masarati, P., Pavel, M. D., Jump, M., and Gennaretti, M., "Adverse Rotorcraft-Pilot Coupling: Recent Research Activities in Europe," 34th European Rotorcraft Forum, Liverpool, UK, September 16–19 2008.

[18] "ARISTOTEL: Aircraft and Rotorcraft Pilot Couplings — Tools and Techniques for Alleviation and Detection," http://www.aristotel.progressima.eu/ (last accessed June 2014).

[19] Pavel, M. D., Malecki, J., DangVu, B., Masarati, P., Gennaretti, M., Jump, M., Smaili, H., Ionita, A., and Zaicek, L., "A Retrospective Survey of Adverse Rotorcraft Pilot Couplings in European Perspective," American Helicopter Society 68th Annual Forum, Fort Worth, Texas, May 1–3 2012.

[20] Mariano, V., Guglieri, G., and Ragazzi, A., "Application of pilot induced oscillations prediction criteria to rotorcraft," American Helicopter Society 67th Annual Forum, Virginia Beach, VA, May 3–5 2011.

[21] Masarati, P., Quaranta, G., and Zanoni, A., "Dependence of helicopter pilots' biodynamic feedthrough on upper limbs' muscular activation patterns," Proc. IMechE Part K: J. Multibody Dynamics, Vol. 227, No. 4, December 2013, pp. 344–362, doi:10.1177/1464419313490680.

[22] "MBDyn: Multibody Dynamics," http://www.mbdyn.org/ (last accessed June 2014).

[23] Masarati, P., Morandini, M., and Mantegazza, P., "An efficient formulation for general-purpose multibody/multiphysics analysis," J. of Computational and Nonlinear Dynamics, Vol. 9, No. 4, 2014, pp. 041001, doi:10.1115/1.4025628.

[24] Masarati, P. and Quaranta, G., "Bioaeroservoelastic Analysis of Involuntary Rotorcraft-Pilot Interaction," J. of Computational and Nonlinear Dynamics, Vol. 9, No. 3, July 2014, pp. 031009, doi:10.1115/1.4025354.

[25] Mayo, J. R., "The Involuntary Participation of a Human Pilot in a Helicopter Collective Control Loop," 15th European Rotorcraft Forum, Amsterdam, The Netherlands, 12–15 September 1989, pp. 81.1–12.

[26] Masarati, P., Quaranta, G., and Jump, M., "Experimental and Numerical Helicopter Pilot Characterization for Aeroelastic Rotorcraft-Pilot Couplings Analysis," Proc. IMechE, Part G: J. Aerospace Engineering, Vol. 227, No. 1, January 2013, pp. 124–140, doi:10.1177/0954410011427662.

[27] Pennestrì, E., Stefanelli, R., Valentini, P. P., and Vita, L., "Virtual musculo-skeletal model for the biomechanical analysis of the upper limb," Journal of Biomechanics, Vol. 40, No. 6, 2007, pp. 1350–1361, doi:10.1016/j.jbiomech.2006.05.013.

[28] Griffin, M. J., Handbook of Human Vibration, Academic Press, London, 1990.

[29] McDowell, M. A., Fryar, C. D., Ogden, C. L., and Flegal, K. M., "Anthropometric Reference Data for Children and Adults: United States, 2003–2006," National Health Statistics Reports n. 10, US Department of Health and Human Services, Centers for Disease Control and Prevention, National Center for Health Statistics, October 22 2008.

[30] Cheverud, J., Gordon, C. C., Walker, R. A., Jacquish, C., Kohn, L., Moore, A., and Yamashita, N., "1988 anthropometric survey of US Army personnel: correlation coefficients and regression equations. Part 1: Statistical Techniques, Landmark, and Mesurement Definitions," TR 90/032, NATICK, 1990.

[31] Cheverud, J., Gordon, C. C., Walker, R. A., Jacquish, C., Kohn, L., Moore, A., and Yamashita, N., "1988 anthropometric survey of US Army personnel: correlation coefficients and regression equations. Part 4: Bivariate Regression Tables," TR 90/035, NATICK, 1990.

[32] Masarati, P., "Computed Torque Control of Redundant Manipulators Using General-Purpose Software in Real-Time," Multibody System Dynamics, in press, doi:10.1007/s11044-013-9377-4.

[33] Stroeve, S., "Impedance characteristics of a neuromusculoskeletal model of the human arm I. Posture control," Biological Cybernetics, Vol. 81, No. 5–6, 1999, pp. 475–494, doi:10.1007/s004220050577.

[34] Zajac, F. E., "Muscle and tendon: properties, models, scaling, and application to biomechanics and motor control," Critical Reviews in Biomedical Engineering, Vol. 17, No. 4, 1989, pp. 359–411.

[35] Venrooij, J., Abbink, D. A., Mulder, M., van Paassen, M. M., and Mulder, M., "Biodynamic feedthrough is task dependent," 2010 IEEE International Conference on Systems Man and Cybernetics (SMC), Istanbul, Turkey, October 10–13 2010, pp. 2571–2578, doi:10.1109/ICSMC.2010.5641915.

[36] Quaranta, G., Masarati, P., and Venrooij, J., "Impact of pilots' biodynamic feedthrough on rotorcraft by robust stability," Journal of Sound and Vibration, Vol. 332, No. 20, September 2013, pp. 4948–4962, doi:10.1016/j.jsv.2013.04.020.

[37] Zanlucchi, S., Masarati, P., and Quaranta, G., "A Pilot-Control Device Model for Helicopter Sensitivity to Collective Bounce," ASME IDETC/CIE 2014, Buffalo, NY, August 17–20 2014, DETC2014-34479.

[38] Skogestad, S. and Postlethwaite, I., Multivariable Feedback Control, John Wiley & Sons, Chichester, 2005.

[39] Szabolcsi, R., "Modeling of the human pilot time delay using Padé series," Academic and Applied Research in Military Science, Vol. 6, No. 3, 2007, pp. 405–428.

[40] Boril, J. and Jalovecky, R., "Effect of the pilot behavior model on the helicopter stability in the auto-stabilization system failure," 2012 IEEE First AESS European Conference on Satellite Telecommunications (ESTEL), 2012, pp. 1–4, doi:10.1109/ESTEL.2012.6400107.

[41] Gray, III, W. R., "Boundary Avoidance Tracking: A New Pilot Tracking Model," AIAA Atmospheric Flight Mechanics Conference and Exhibit, San Francisco, California, August 15–18 2005, AIAA 2005-5810 doi:10.2514/6.2005-5810.

[42] Brinkerink, N. and Pavel, M. D., "Capturing the switch between point tracking and boundary avoiding pilot behaviour in a PIO event," Rotorcraft Handling Qualities Conference, Liverpool, UK, November 4–6 2008.

[43] Padfield, G. D., Lu, L., and Jump, M., "Tau Guidance in Boundary-Avoidance Tracking - New Perspectives on Pilot-Induced Oscillations," J. of Guidance, Control, and Dynamics, Vol. 35, No. 1, 2012, pp. 80–92, doi:10.2514/1.54065.

[44] Ockier, C. J., "Pilot induced oscillations in helicopters — Three case studies," Tech. Rep. IB 111-96/12, German Aerospace Center (DLR), Braunschweig, Germany, 1996.

[45] Zhou, S., Lawson, D. L., Morrison, W. E., and Fairweather, I., "Electromechanical delay in isometric muscle contractions evoked by voluntary, reflex and electrical stimulation," European Journal of Applied Physiology and Occupational Physiology, Vol. 70, No. 2, 1995, pp. 138–145, doi:10.1007/BF00361541.

[46] Masarati, P., Quaranta, G., Lu, L., and Jump, M., "A Closed Loop Experiment of Collective Bounce Aeroelastic Rotorcraft-Pilot Coupling," Journal of Sound and Vibration, Vol. 333, No. 1, January 2014, pp. 307–325, doi:10.1016/j.jsv.2013.09.020.

[47] Muscarello, V., Masarati, P., and Quaranta, G., "Multibody Analysis of Rotorcraft-Pilot Coupling," 2nd Joint International Conference on Multibody System Dynamics, edited by P. Eberhard and P. Ziegler, Stuttgart, Germany, May 29–June 1 2012.

[48] Gennaretti, M., Serafini, J., Masarati, P., and Quaranta, G., "Effects of Biodynamic Feedthrough in Rotorcraft-Pilot Coupling: Collective Bounce Case," J. of Guidance, Control, and Dynamics, Vol. 36, No. 6, 2013, pp. 1709–1721, doi:10.2514/1.61355.

[49] Ghiringhelli, G. L., Masarati, P., and Mantegazza, P., "A Multi-Body Implementation of Finite Volume Beams," AIAA Journal, Vol. 38, No. 1, January 2000, pp. 131–138, doi:10.2514/2.933.

[50] Padfield, G. D., Helicopter Flight Dynamics: The Theory and Application of Flying Qualities and Simulation Modelling, Blackwell Publishing, 2007.

[51] Anonymous, "Performance Specification, Handling Qualities Requirements for Military Rotorcraft," ADS 33-E-PRF, US Army AMCOM, Redstone, Alabama, 2000.

[52] Muscarello, V., Quaranta, G., and Masarati, P., "The Role of Rotor Coning in Helicopter Proneness to Collective Bounce," Aerospace Science and Technology, Vol. 36, July 2014, pp. 103–113, doi:10.1016/j.ast.2014.04.006.